JOURNAL OF MATERIALS SCIENCE 21 (1986) 1429–1435

Sinterability of various high-purity magnesium oxide powders

KIYOSHI ITATANI, MASAYUKI NOMURA, AKIRA KISHIOKA, MAKIO KINOSHITA
Department of Chemistry, Faculty of Science and Technology, Sophia University, Tokyo 102, Japan

The sinterability of high-purity MgO powders with different production histories was investigated to make clear the relationship between the powder characterization, the densification processes, and the changes in microstructure both with increasing temperature at a rate of 10° C min^{-1} and at a fixed temperature of 1450° C for 5 h. The densification behaviour and the changes in microstructure of these compressed bodies were affected chiefly by their original surface activity and degree of agglomeration, depending on the production histories: (i) the ultra-fine and well-dispersed powder prepared by the vapour-phase oxidation process showed that densification proceeded with an appreciable grain growth with few closed pores remaining; (ii) powder derived from the sea-water magnesia process showed that the densification behaviour was affected by the species of magnesium salt, i.e. basic magnesium carbonate or magnesium hydroxide, used as a precursor; however, whichever magnesium salt was used, its sintered compact showed similar closed porosities and grain-size distributions; (iii) powder derived from the spark-discharge process contained skeletons of the original $Mg(OH)_2$ particles; however, the densification proceeded gradually with slow grain growth, reflecting the fact that the powder has a moderate surface area (36 m^2 g^{-1}). The sintered compact from (iii) had a small closed porosity and the smallest grain-size distribution among the compacts used in this investigation.

1. Introduction

As magnesium oxide (MgO) powder is generally prepared by decomposing magnesium salt, its sinterability is strongly affected by what kind of magnesium compound is used as a precursor [1–5]: MgO powders derived from carbonate, acetate, and hydroxide are easily sinterable, whereas those derived from chloride, nitrate and sulphate make the sintering difficult. In practice, most of the commercial MgO powders are obtained by the sea-water magnesia process (SWM–P) [6]: MgO is prepared by the decomposition of $Mg(OH)_2$ which is precipitated by introducing $Ca(OH)_2$ into sea-water or some magnesium-containing solution. In the conventional SWM–P, however, the purity of MgO powder has been limited to about 96 to 98%, because even slight amounts of impurities tend to coprecipitate when $Mg(OH)_2$ is formed. The refinement of this MgO powder has proceeded by reducing the impurities, and MgO powder whose purity exceeds 99.9% has become available in recent years.

New practical processes have also been developed for preparing high-purity MgO powders: (i) a vapour-phase oxidation process (VPO–P) [7] and (ii) a spark-discharge process (SD–P) [8]. In the former process, the vaporized magnesium metal is oxidized directly to form MgO, while in the latter process $Mg(OH)_2$, prepared by discharging between magnesium pellets in high-purity water, is decomposed to form MgO. These MgO powders are more than 99.9% pure; moreover, the properties of the commercial powders are also clarified in detail by the manufacturers. Although these high-purity MgO powders are produced chiefly for use as sintering materials, their sinterabilities have not been yet examined in detail.

The present authors have studied the effects of metal phosphate additions on the sintering of MgO [9–13]; however, more information on the sinterability of the pure MgO powder is required to work out the effect of phosphate additives. In this paper, we investigate the densification behaviour and changes in the microstructure of the above high-purity MgO powders. Furthermore, the sinterability of these MgO powders is systematically evaluated.

2. Experimental details

2.1. Materials

The four kinds of commercial MgO powder (> 99.9% pure) are designated by A, B, C, and D in this paper. Details of their production histories are shown in Table I. Powder A was produced by direct oxidation of the magnesium vapour. Powder B was obtained by decomposing basic magnesium carbonate resulting from the carbonation of $Mg(OH)_2$. Powders C and D were prepared by the decomposition of $Mg(OH)_2$ to MgO.

0022–2461/86 $03.00 + .12

TABLE I Production histories of MgO powders

Powder	Process	Parent crystal	Calcination	Grinding
A	VPO–P	–	–	No
B	SWM–P	Basic magnesium carbonate	800° C, 1 h	Yes
C	SD–P	$Mg(OH)_2$	900° C, 4 h	No
D	SWM–P	$Mg(OH)_2$	900° C, 1 h	Yes

2.2. Measurements of specific surface area and particle size and observation of morphology

Specific surface areas of MgO powders were measured by the BET technique (BET–T), using N_2 as an adsorption gas. Particle sizes were measured on the basis of BET–T and the X-ray diffraction technique (XRD–T). The particle size (G_{BET}) derived from BET was calculated from the following expression:

$$G_{BET} = \frac{F}{\varrho S} \quad (1)$$

where F represents a particle-shape factor ($F = 6$, assuming it to be cubic), ϱ the powder density and S the specific surface area.

On the other hand, the particle size (G_{XRD}) derived from XRD–T was obtained by the following expression:

$$G_{XRD} = \frac{K\lambda}{\beta \cos\theta} \quad (2)$$

where λ represents the wavelength of Cu$K\alpha_1$, K is a shape factor ($= 0.9$), β the half-height width of the (4 2 0) reflection of MgO, and θ the Bragg angle.

To evaluate the degree of agglomeration of particles, the particle-size distribution of a powder was measured by centrifugal sedimentation, using ethyl alcohol as a dispersion medium.

The morphologies of particles were observed by transmission electron microscopy (TEM), using a Hitachi Model H–300.

2.3. Preparation of compacts

The four kinds of powder (A, B, C, and D) were pressed in the following manner: about 0.15 g of MgO powder was pressed at 294 MPa into a disc of 5 mm diameter and 3 mm height, while about 2.50 g of MgO powder was pressed at 90 MPa into a disc of 20 mm diameter and 4 mm height. The former was used for the measurement of shrinkage and the latter for measurements of relative density and grain size.

2.4. Measurement of shrinkage with increasing temperature

The shrinkages of MgO compacts were measured by using a dilatometer (Model 8096 B1 from Rigaku, Tokyo). Compacts were heated from room temperature up to 1450° C at a rate of 10° C min^{-1} in air. A sintered alumina rod (5 mm diameter and 3 mm height) was used as a standard substance.

2.5. Measurements of relative density and porosity

Compacts were heated up at a rate of about 500° C h^{-1} and were sintered at 1450° C for 5 h. They were then annealed overnight in a furnace.

The relative density (D_{Rela}) before and after sintering a compact was obtained by the following equation:

$$D_{Rela} = 100 \frac{D_{Bulk}}{D_{Theo}} \quad (3)$$

where D_{Theo} is the theoretical density and D_{Bulk} is the bulk density of the compact. Here the bulk density was calculated by measuring the weight and dimensions of the sintered compact, whereas the theoretical density was calculated from the lattice parameters of MgO obtained by using XRD–T.

The total porosity P_{Total}, the open porosity P_{Open}, and the closed porosity P_{Closed} were measured by the same technique as that of Deacon [14], who used CCl_4 as a replacement liquid. The relationship between the porosities was as follows:

$$P_{Total} = 100 \left(1 - \frac{D_{Bulk}}{D_{True}}\right) \quad (4)$$

$$P_{Open} = 100 \left(1 - \frac{D_{Bulk}}{D_{App}}\right) \quad (5)$$

$$P_{Closed} = 100 D_{Bulk} \left(\frac{1}{D_{App}} - \frac{1}{D_{True}}\right) \quad (6)$$

where D_{True} is the true density and D_{App} the apparent solid density.

2.6. Microstructure observations of sintered compacts

Microstructures of sintered compacts were observed by scanning electron microscopy (SEM) using a Hitachi Model S–430, after thermal etching of the polished surfaces. From these SEM photographs, grain sizes were obtained by the application of Fullman's correction to the measured values [15]: after test lines were drawn at regular intervals, particle sizes were obtained by multiplying by $\pi/2$ the measured values of the distance between grain boundaries on the lines. About 400 to 500 grains were counted in each measurement.

3. Results and discussion

3.1. Characterization of starting materials

The properties of sintered compacts are strongly affected by those of the starting material [16]: purity, kind and quantity of impurity, particle shape and size, surface area, etc. In addition, the production history of the powder, i.e. the kind of parent crystal used, and its calcination temperature and time, affect the properties of the sintered compact [5]. In this section, we will discuss powder characterization from the viewpoints of production history, impurities, and particle shape and size.

TABLE II Analyses of MgO powders (wt %) from manufacturers' catalogues

Compound	Powder			
	A	B	C	D
MgO	99.98	> 99.95	> 99.9	99.9
CaO	0.004	< 0.01		0.002
SiO_2	0.002	< 0.01	0.0073	0.002
Al_2O_3		0.003	0.0045	0.002
Fe_2O_3	0.002	0.003	0.0029	0.003
Na_2O	0.007		0.001	0.007
B_2O_3				0.0006
Cr_2O_3	0.0005			0.0002
MnO			0.0062	0.0013

3.1.1. Production history

As shown in Table I, Powder A was prepared by VPO–P, i.e. the direct oxidation of magnesium vapour. Powders B and D were produced by SWM–P, while Powder C was prepared by SD–P. Although Powders C and D were obtained by the direct decomposition of $Mg(OH)_2$, Powder B was prepared by decomposing the basic magnesium carbonate derived from $Mg(OH)_2$; such a second-step process was employed to improve the purification of MgO.

Except for Powder A (prepared by VPO–P), MgO powders are obtained by decomposing magnesium compounds. Clearly, the densification of the MgO compact is affected by what kind of magnesium compound is used as a precursor; this is because the porosity inhomogeneties tend to occur in a green compact if the skeletons, formed by the decomposition of a parent crystal, consist of strongly-bonded MgO crystals or hard aggregates [17]. Once such pores are formed, they cannot easily be filled in during sintering [18, 19]. As MgO powders derived from carbonate and hydroxide are known to be easily sinterable [5, 16] their skeletons seem to be composed of weakly-bonded MgO crystals.

3.1.2. Impurity

The impurity contents of each MgO powder are listed in Table II; the data are quoted from the catalogues of the manufacturers. The major impurities were Na_2O in Powder A, Al_2O_3 and Fe_2O_3 in Powder B, SiO_2 in Powder C, and Na_2O in Powder D.

Whether the effects of the above impurities can be described or not depends on their quantity and their state of segregation [20]. Unfortunately, the amounts of these impurities are too small to confirm their effects on the sintering of MgO.

3.1.3. Surface area, particle size and shape

Table III shows the specific surface area and particle sizes of the sample powders. Here G_{BET} can be defined as a primary-particle size [21]; a primary particle does not always consist of a single crystal but often of several crystallites whose average size can be defined as G_{XRD}.

TABLE III Properties of MgO powders

Powder	Specific surface area ($m^2\ g^{-1}$)	G_{XRD} (nm)	G_{BET} (nm)	$\frac{G_{BET}}{G_{XRD}}$
A	149.8	11.2	11.2	1.00
B	51.8	22.2	32.3	1.45
C	36.0	27.5	46.5	1.69
D	27.1	32.2	61.9	1.92

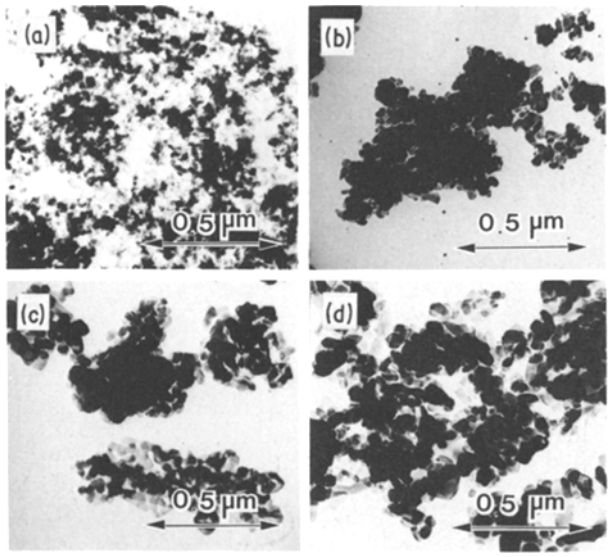

Figure 1 TEM photographs of MgO powders: (a) Powder A, (b) Powder B, (c) Powder C, (d) Powder D.

The specific surface areas were arranged in the following order: A > B > C > D. Conversely, the magnitudes of the primary-particle size and crystallite size were in the order D > C > B > A. Furthermore, the D_{BET}/D_{XRD} ratios were in the order D > C > B > A.

The powder activity which provides the driving force for sintering increases generally with increasing surface area, in other words with decreasing particle size. Moreover, a smaller value of D_{BET}/D_{XRD} indicates that the primary particle is composed of softer agglomerations of crystallites [22].

Thus Powder A is expected to have the highest surface activity and the softest agglomeration of crystallites among the four powders.

Fig. 1 shows TEM photographs of the four powders. The particles in Powder A appeared to be cubic, roughly 10 nm in size; the particles were well dispersed and little agglomeration was observed. The particles in Powder B were polyhedral with rounded corners and were roughly 25 nm in size; they appeared to form clusters. Nevertheless, such a cluster may be composed chiefly of weakly-bonded MgO crystals, judging from which MgO powders derived from carbonate are easily sinterable. The particles in Powder C were observed to have hexagonal and polyhedral shapes and to be about 50 nm in size; parts of the skeletons of the parent crystals seem to remain. Particles in Powder D had hexagonal and polyhedral shapes and were about 65 nm in size.

On the whole, the average particle sizes in Fig. 1 are in accord with those obtained by BET–T. This agreement indicates that the particles have smooth surfaces with few cracks and that they almost correspond to the primary particles [21].

Fig. 2 shows the particle-size distributions of the four powders. Here the "particle" can be interpreted as an agglomerate [19]. The distribution of particle

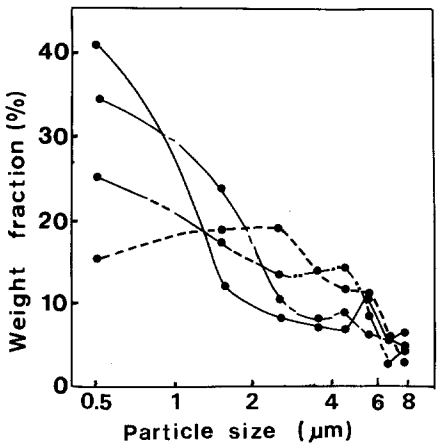

Figure 2 "Particle" size distributions of MgO powders: (——) Powder A, (– – –) Powder B, (–·–) Powder C, (– – – –) Powder D.

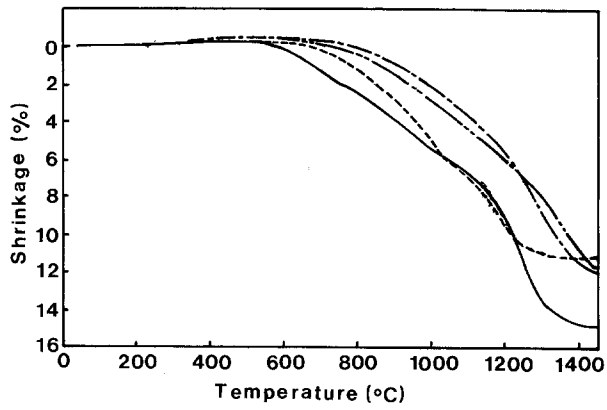

Figure 3 Shrinkage curves for MgO compacts at heating rate of 10° C min^{-1}. (——) Powder A, (– – –) Powder B, (– – –) Powder C, (– – – –) Powder D.

sizes in Powder A was similar to those in Powders C and D; about 40 wt % in Powder A was occupied by particles of average size 0.5 μm, whereas the percentage of this particle size decreased down to about 35 wt % in Powder C and down to about 25 wt % in Powder D. The particle-size distribution curve in Powder B was quite different from those in Powders A, C, and D: it showed a peak at 2.5 μm. The average particle size was 2.5 μm in Powder A, 3.2 μm in Powder B, 2.4 μm in Powder C and 2.9 μm in Powder D. Comparing these results with those shown in TEM photographs (Fig. 1) without making any assumptions, an agglomerate is composed of roughly 250 primary particles in Powder A, 130 particles in Powder B, 48 particles in Powder C and 44 particles in Powder D. These results shows that the smaller particles tend to gather to form an agglomerate because of the adhesion between them.

3.2. Sintering behaviour with increasing temperature

The characteristics of the four powders have already been clarified in Section 3.1. The major factors which affect the sintering behaviour seem to be the surface activity and the degree of agglomeration, depending on the production history. Based on this information, the compacts of each powder are investigated from the viewpoints of the densification process and the change in the microstructure with increasing temperature.

3.2.1. Shrinkage

The densification behaviour of the four compressed powders was examined by using a dilatometer. The results are shown in Fig. 3. The densification of Compact A began at about 600° C and was accelerated above 1100° C. The densification of Compact B began at about 700° C and proceeded rapidly up to about 1300° C; however, it stopped on further heating up to 1450° C. Compact C began to densify at about 700° C and proceeded gradually up to 1450° C. The densification of Compact D proceeded faster than that of Compact C up to about 1200° C; however, on further beating, Compact C began to show densification more rapidly than Compact D.

The temperature at which the densification began to show shifted to the higher-side in the following order: A < B < D < C. The initial sintering of Compacts A and B seems to be chiefly due to the surface activity which is provided by the huge surface areas of their starting powders. Taking only the surface activity due to the surface area into account, Compact D should change places with Compact C; however, it can be reasonably explained by considering that the surface activity in Compact D is partly raised by the breakdown of the skeletons by grinding [23]. Such a high surface activity will be lost by rapid grain growth as the temperature increases, so that the densification of Compact D proceeds more slowly than that of Compact C.

3.2.2. Grain growth

As typical cases, two kinds of SEM photograph are illustrated here. Fig. 4 shows SEM photographs of compacts heated at 1200° C. The average grain sizes in Compacts A, C and D were roughly 0.3 μm, while that in Compact B was roughly 0.5 μm. In contrast with the porous surface on Compact D, the grains in Compact B were arranged in close packing, reflecting the fact that Compact B was in the final stage of sintering

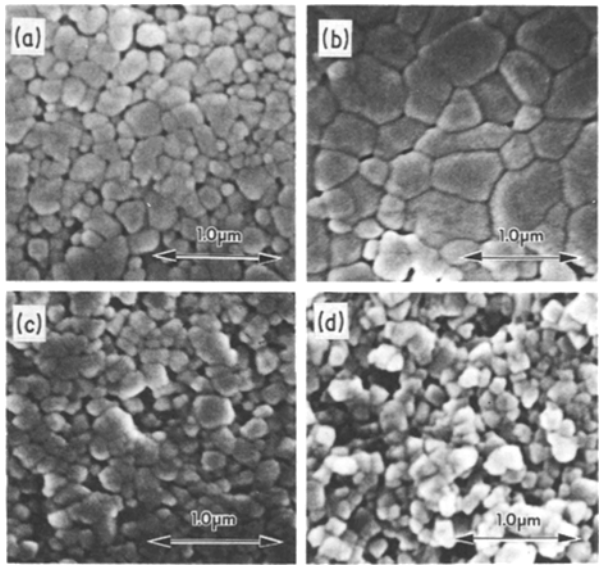

Figure 4 SEM photographs of polished surfaces of MgO compacts sintered at 1200° C (heating rate 10° C min^{-1}). (a) Compact A, (b) Compact B, (c) Compact C, (d) Compact D.

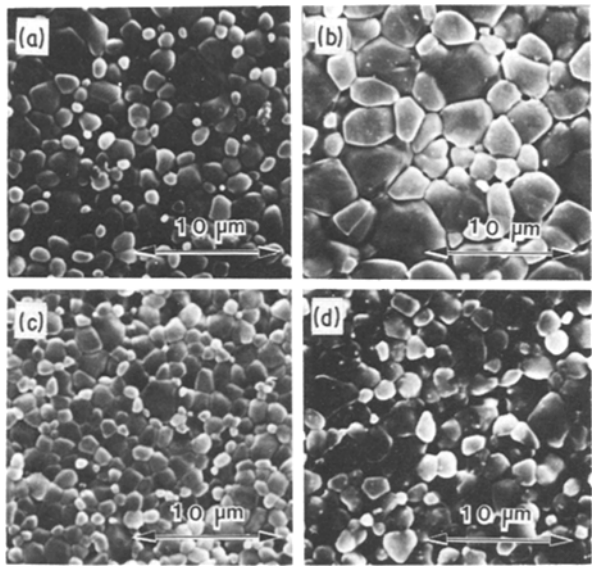

Figure 5 SEM photographs of polished surfaces of MgO compacts sintered at 1400° C (heating rate 10° C min^{-1}). (a) Compact A, (b) Compact B, (c) Compact C, (d) Compact D.

at this temperature. The rapid grain growth in Compact B may be brought about by an active mass transfer due to the high surface activity and soft agglomeration.

Fig. 5 shows SEM photographs of compacts heated at 1400° C. The average grain sizes in Compacts A, C and D were roughly 1 to 3 μm, while that in Compact B was roughly 3 to 5 μm. The grains grew three to ten times as large as those at 1200° C. Despite the rapid grain growth in these powders, however, few pores were present in the interiors of the grains. It is expected that most of the pores in these four compacts can be eliminated without trapping in the grains.

Fig. 6 shows the changes in the grain-size distributions of these compacts heated at 1000, 1200, 1300 and 1400° C. In addition, Fig. 7 shows the average grain sizes of these compacts, obtained by calculation from the results shown in Fig. 6. The overall trend indicated from Fig. 6 is that the grains grew rapidly as their distributions widened. The magnitudes of the average

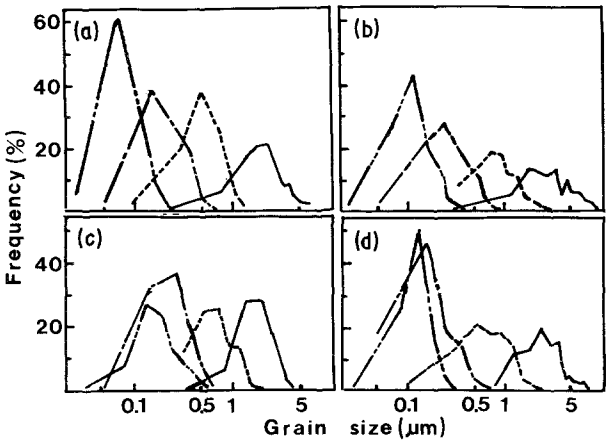

Figure 6 Changes in grain-size distribution of MgO compacts sintered at (– – –) 1000, (– – –) 1200, (– – –) 1300 and (——) 1400° C (heating rate 10° C min^{-1}). (a) Compact A, (b) Compact B, (c) Compact C, (d) Compact D.

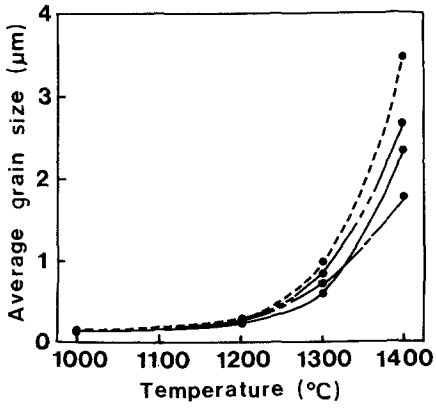

Figure 7 Changes in grain growth of MgO compacts (heating rate 10° C min^{-1}). (——) Powder A, (– – –) Powder B, (– – –) Powder C, (– – –) Powder D.

grain sizes in each compact at 1300° C were related as follows: B > D > C > A; at 1400° C, the order was changed and became B > D > A > C. Compact A changed places with Compact C at 1400° C, which suggests that grain growth in Compact A is strongly accelerated above 1300° C; the adhesion of grains may be promoted by the active mass transfer whose driving force still remains at this temperatures. Compacts B and D exhibit appreciable grain growth.

Judging from the fact that their original powders are prepared by SWM–P, it is probable that the properties as well as the grain growth in a compact depend chiefly on the production history of the original powder. Furthermore, the grains in Compact C grew slower than those of other compacts, probably because of the soft agglomeration and the slow migration of grain boundaries, which is brought about by the moderate surface area (36 m^2 g^{-1}).

From the results of both densification behaviour and grain growth, the following relations are found in the temperature range 1000 to 1400° C: (i) a continuous grain growth in the case of Compacts A, C, and D proceeds with increasing densification, and (ii) a marked grain growth in Compact B occurs successively, even after the densification stops. The behaviour shown may in both cases reflect the properties of the original powders, especially the surface activity and degree of agglomeration.

3.3. Sintering behaviour at constant temperature

In the previous section, four kinds of MgO compact were examined to make clear the relationship between the densification behaviour and the grain growth. In this section, further investigation of the densification and the microstructure at constant temperature is carried out to confirm whether the results are in accord with those obtained with increasing temperature.

3.3.1. Densification

Fig. 8 shows the relative densities of the four compacts heated at 1450° C for 5 h. The green relative densities of these compacts are also illustrated in the figure. The magnitudes of the green relative densities were related

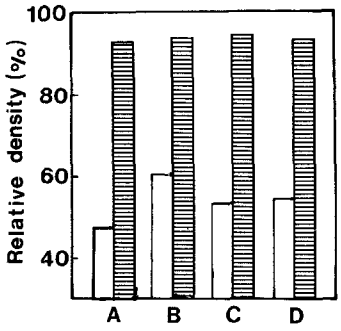

Figure 8 Relative densities of MgO compacts (□) before and (▤) after sintering at 1450° C for 5 h.

as follows: B > D > C > A. The fact that Powder B showed a good compactivity suggests that it is composed of "clusters" formed as a result of the large contact areas between particles. The green relative density of Compact A was the lowest of the four compacts; the powder resists compaction due to the bridging between particles. Thus, it is found that the large densification, about 15% of the shrinkage shown in Fig. 3, is brought by the low green relative density. In spite of the variation in green relative densities of these four compacts, there was not much difference among them in sintered relative density; they were all about 95% of the theoretical densities.

Fig. 9 shows the total, open, and closed porosities of these compacts. The total porosities can be arranged in the order D > A > B > C. The closed porosity could be classified more clearly than the open porosity; the closed porosities in these sintered compacts were divided into two groups, i.e. (i) Compacts A and C and (ii) Compacts B and D.

The pores which are open to the outside of the compact can easily be removed along grain boundaries. However, once the pores are isolated from the boundaries, their removal is only possible by the migration of vacancies from the surfaces of the pores to and along the grain boundaries [24]. Consequently, the pores far from the grain boundaries will disappear more slowly than those on the boundaries. For this reason, the magnitude of the closed porosity plays an important role in controlling the ultimate sintered density.

Comparing the results for the closed porosity with those for the grain growth in Fig. 7, it is found that Compacts B and D, whose porosities are higher than

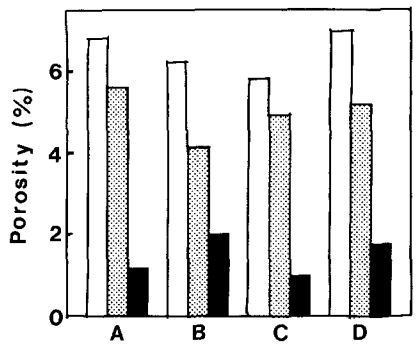

Figure 9 Porosities of MgO compacts sintered at 1450° C for 5 h. (□) Total porosity, (▨) open porosity, (■) closed porosity.

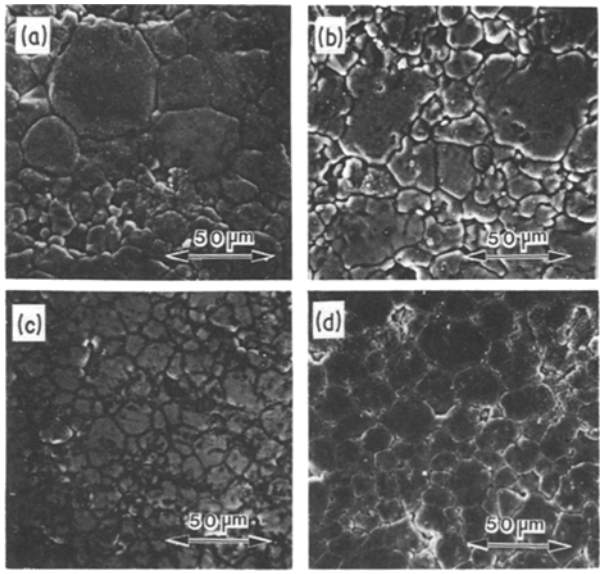

Figure 10 SEM photographs of polished surfaces of MgO compacts sintered at 1450° C for 5 h. (a) Compact A, (b) Compact B, (c) Compact C, (d) Compact D.

for Compacts A and C, show rapid grain growth at increasing temperatures. This fact indicates that a rapid grain growth brings about the entrapment of pores. Thus, it seems that the grains grow slowly in reducing the closed pores.

3.3.2. Microstructure

Fig. 10 shows SEM photographs of four compacts heated at 1450° C for 5 h. The polished surface of Compact A showed that smaller grains were present between larger grains; such a grain growth may occur because of microvariations in green density, reflecting the fact that the compression pressure is not completely transmitted throughout the compact due to bridging between the ultrafine particles. Compact B revealed a discontinuous grain growth; pores were present on and within grain boundaries. Based on the fact that few pores were observed within the grains with increasing temperatures, these pores may be trapped by the rapid migration of grain boundaries during heating at 1450° C for 5 h. The microstructure of Compact C is similar to that of Compact D; the grains were hexagonal in shape and were 10 to 20 μm in size. Their grain boundaries met each other at an angle of about 120°, suggesting that Compacts C and D were in the final stage of sintering [25].

Fig. 11 shows the grain-size distributions of the four sintered compacts. These four kinds of compact showed normal distributions; the average grain size was 30.2 μm in Compact A, 22.8 μm in Compact B, 13.7 μm in Compact C and 18.9 μm in Compact D.

Clearly, the grains in Compact A grow the largest. Considering the fact that the average grain size of Compact A was smaller than that of Compact D at 1400° C (Fig. 7), the grains seem to grow rapidly without a break during heating at 1450° C for 5 h. The distribution of grain size in Compact B is similar to that in Compact D; it is inferred that such an agreement may be due to the similarity in production history. Furthermore, the grain size in Compact C

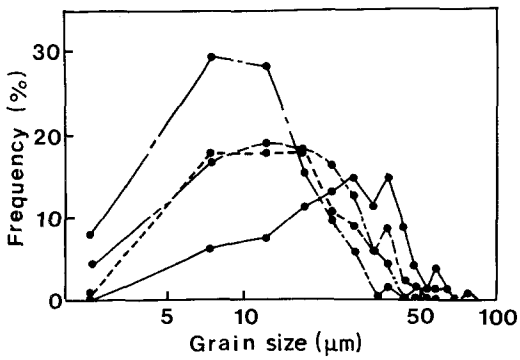

Figure 11 Grain-size distributions of MgO compacts sintered at 1450° C for 5 h. (——) Compact A, (– – –) Compact B, (– · –) Compact C, (– · · –) Compact D.

remains the smallest among the four compacts; grain growth may be retarded by the slow migration of the grain boundaries, probably because the starting powder has moderate surface activity and consists of soft agglomerates.

As mentioned above, the sinterabilities of the high-purity MgO powders examined in this paper can be divided into three groups: (i) Powder A, (ii) Powders B and D, and (iii) Powder C. The differences between the sinterabilities seem to be attributable to the production history, which affects chiefly the surface activity and the degree of agglomeration. Here, a slight change in the preparation conditions may not affect the sintering substantially if the production process is the same.

4. Conclusion

The sinterability of high-purity MgO powders with different production histories was investigated systematically to relate the powder characterization with the densification behaviour and with the change in microstructures when heated at increasing temperature (heating rate $10^\circ C\,min^{-1}$) and at constant temperature (1450° C, 5 h).

The sinterabilities of these compressed bodies were affected chiefly by their original surface activities and degree of the agglomeration, which depended on the production history. The relationships among these factors were characterized as follows:

1. The ultrafine powder prepared by the vapour-phase oxidation process showed that the densification of the compressed body proceeded rapidly with an appreciable grain growth; however, few closed pores remained in the sintered compact because the original powder consisted of well-dispersed particles.

2. The initial and intermediate stages of the sintering of the powder prepared by the sea-water magnesia process were clearly affected by what kind of magnesium compound, i.e. basic magnesium carbonate or magnesium hydroxide, was used as a precursor; however, when the compact was sintered to the final stage, they gave similar closed porosities and grain-size distributions.

3. The powder prepared by the spark-discharge process revealed that the densification proceeded gradually, with slow grain growth. The sintered compact showed a small closed porosity and the smallest grain-size distribution among the compacts examined in this investigation.

The aim of this paper was to clarify the relationship between the properties of the starting materials and those of the sintered compacts. For this reason, the authors did not refer to the ultimate sintered density of each compact; however, it is expected that MgO compacts used in this investigation can attain nearly zero porosity by the selection of sintering conditions suitable for individual cases.

Acknowledgements

The authors wish to thank Mr Koji Ioku for performing some experiments, and Ube industries Ltd and Ube Chemical Industries Ltd for providing two of the sample powders.

References

1. D. T. LIVEY, B. M. WANKLYN, M. H. HEWITT and P. MURRAY, *Trans. Br. Ceram. Soc.* **56** (1957) 217.
2. W. H. RHODES and B. J. WENCH, *J. Amer. Ceram. Soc.* **56** (1973) 495.
3. S. M. ZUBAKOV, P. N. BABIN and A. Kh. AKISHEV, *Ogneupory* No. 5 (1979) 47.
4. E. V. IVANOV, V. P. BUNINA, G. Z. DOLGINA and V. S. SHAPOVALOV, *ibid.* No. 7 (1979) 41.
5. K. HAMANO and S. KATAFUCHI, *Taikabutsu* **32** (1980) 243.
6. J. GREEN, *J. Mater. Sci.* **18** (1983) 637.
7. T. WATARI, K. NAKAYOSHI and A. KATO, paper presented at Spring Meeting, The Japan Society of Powder and Powder Metallurgy, Kyoto, Japan, May 23 1984 (Nippon Kagaku Kaishi, 1985) p. 790.
8. W. ISHIBASHI, T. ARAKI, K. KISHIMOTO and H. KUNO, *Bull. Ceram. Soc. Jpn.* **6** (1971) 461.
9. M. KINOSHITA and K. ITATANI, *Yogyo-Kyokai-Shi* **88** (1980) 388.
10. *Idem, ibid.* **90** (1982) 463.
11. *Idem, ibid.* **90** (1982) 570.
12. K. ITATANI, A. KISHIOKA and M. KINOSHITA, *ibid.* **92** (1984) 530.
13. K. ITATANI, T. YAMAMOTO, A. KISHIOKA and M. KINOSHITA, *Amer. Ceram. Soc. Bull.* **64** (1985) 1124.
14. R. F. DEACON, S. F. A. MISKIN and B. J. LADELL, *Trans. Br. Ceram. Soc.* **65** (1966) 585.
15. R. L. FULLMAN, *Trans. AIME* **197** (1953) 447.
16. K. HAMANO, *Bull. Ceram. Soc. Jpn.* **7** (1972) 231.
17. F. W. DYNYS and J. W. HALLORAN, *J. Amer. Ceram. Soc.* **66** (1983) 655.
18. M. D. SACKS and J. A. PASK, *ibid.* **65** (1982) 655.
19. F. W. DYNYS and J. W. HALLORAN, *ibid.* **67** (1984) 596.
20. J. GREEN and E. DE ROEVER, *Taikabutsu* **35** (1983) 249.
21. T. YAMAGUCHI, in "Ceramic Processing: Powder Preparation and Forming" (Ceramic Society of Japan, Tokyo, 1984) p. 122.
22. A. M. M. GADALLA and H. W. HENNICKE, *Powder Met. Int.* **5** (1973) 196.
23. K. YAMAMOTO and K. UMEYA, *Amer. Ceram. Soc. Bull.* **60** (1981) 636.
24. J. E. BURKE, *J. Amer. Ceram. Soc.* **40** (1957) 80.
25. K. HAMANO and H. KAMIZONO, *Yogyo-Kyokai-Shi* **85** (1977) 390.

Received 13 May
and accepted 12 June 1985